Sensitivity and identifiability of hydraulic and geophysical parameters from streaming potential signals in unsaturated porous media

Anis Younes[1,2,3], Jabran Zaouali[1], Francois Lehmann[1], Marwan Fahs[*,1]

[1]LHyGES, Université de Strasbourg/EOST/ENGEES, CNRS, 1 rue Blessig, 67084 Strasbourg, France.
[2] IRD UMR LISAH, F-92761 Montpellier, France
[3] LMHE, ENIT, Tunis, Tunisie

Submitted to: Hydrology-and-Earth-System-Sciences

* Contact person: Marwan Fahs
E-mail: fahs@unistra.fr

Abstract

Fluid flow in a charged porous medium generates electric potentials called Streaming potential (SP). The SP signal is related to both hydraulic and electrical properties of the soil. In this work, Global Sensitivity Analysis (GSA) and parameter estimation procedures are performed to assess the influence of hydraulic and geophysical parameters on the SP signals and to investigate the identifiability of these parameters from SP measurements. Both procedures are applied to a synthetic column experiment involving a falling head infiltration phase followed by a drainage phase.

GSA is used through variance-based sensitivity indices, calculated using sparse Polynomial Chaos Expansion (PCE). To allow high PCE orders, we use an efficient sparse PCE algorithm which selects the best sparse PCE from a given data set using the Kashyap Information Criterion (KIC). Parameter identifiability is performed using two approaches: the Bayesian approach based on the Markov Chain Monte Carlo (MCMC) method and the First-Order Approximation (FOA) approach based on the Levenberg Marquardt algorithm. The comparison between the two approaches allows to check whether FOA can provide reliable estimation of parameters and associated uncertainties for the investigated highly nonlinear hydrogeophysical problem.

GSA results show that at short times, the saturated hydraulic conductivity (K_S) and the voltage coupling coefficient at saturation (C_{sat}) are the most influential parameters, whereas, at long times, the residual water content (θ_r), the Mualem-van Genuchten parameter (n) and the Archies's saturation exponent (n_a) become influential with strong interactions between them. The Mualem-van Genuchten parameter (α) has a very weak influence on the SP signals during the whole experiment.

Results of parameter estimation show that, although the studied problem is highly nonlinear, when several SP data collected at different altitudes inside the column are used to calibrate the model, all hydraulic (K_S, θ_r, α and n) and geophysical (n_a and C_{sat}) parameters can be reasonably estimated from the SP measurements. Further, in this case, the FOA approach provides accurate estimations of both mean parameter values and uncertainty regions. Conversely, when the number of SP measurements used for the calibration is strongly reduced, the FOA approach yields accurate mean parameter values (in agreement with MCMC results) but inaccurate and even unphysical confidence intervals for parameters with large uncertainty regions.

Keywords

Drainage experiment, Streaming Potential, Global Sensitivity Analysis, Markov chain Monte Carlo, parameter estimation.

1. Introduction

Flow through a charged porous medium can generate an electric potential (Zablocki, 1978; Ishido and Mizutani, 1981; Allegre et al., 2010; Jougnot and Linde, 2013), called Streaming Potential (SP). The SP signals play an important role in several applications related to hydrogeology and geothermal reservoir engineering as they are useful for examining subsurface flow dynamics. During the last decade, surface SP anomalies have been widely used to estimate aquifers hydraulic properties (Darnet et al., 2003). Interest on SP is motivated by its low–cost and high sensitivity to water flow. Either coupled or uncoupled approaches can be used for hydraulic parameter estimation from SP signals (Mboh et al., 2012). In the uncoupled approach, Darcy velocities (e.g., Jardani et al., 2007; Bolève et al., 2009) are obtained from tomographic inversion of SP signals and then used for the calibration of the hydrologic model. In the coupled approach, anomalies related to the tomographic inversion are avoided by inverting the full coupled hydrogeophysical model (Hinnell et al., 2010).

The SP signals have been widely studied in saturated porous media (Bogoslovsky and Ogilvy, 1973; Patella, 1997; Sailhac and Marquis, 2001; Richards et al., 2010; Bolève et al., 2009, among others). Fewer studies focused on the application of the SP signal in unsaturated flow despite the big interest for such nonlinear problems (Linde et al., 2007; Allegre et al., 2010; Mboh et al., 2012; Jougnot and Linde, 2013). Hence, in this work we are interested in the SP signals in unsaturated porous media. Our main objective is to investigate the usefulness of the SP signals for the characterization of soil parameters. To this aim, we evaluate the impact of uncertain hydraulic and geophysical parameters on the SP signals and assess the identifiability of these parameters from the SP measurements.

The impact of soil parameters on SP signals is investigated using Global Sensitivity Analysis (GSA). This is a useful tool for characterizing the influential parameters that contribute the

most to the variability of model outputs (Saltelli et al.,1999; Sudret, 2008) and for understanding the behavior of the modeled system. GSA has been applied in several areas, as for risk assessment for groundwater pollution (e.g., Volkova et al., 2008), non-reactive (Fajraoui et al., 2011) and reactive transport experiments (Fajraoui et al., 2012; Younes et al., 2016), for unsaturated flow experiments (Younes et al., 2013), natural convection in porous media (Fajraoui et al., 2017) and seawater intrusion (Rajabi et al., 2015; Riva et al., 2015). To the best of our knowledge, GSA has never been used for SP signals in unsaturated porous media. Hence, in the first part of this study, GSA is performed on a conceptual model inspired from the laboratory experiment of Mboh et al. (2012) where SP signals are measured at different altitudes in a sandy soil column during a falling-head infiltration phase followed by a drainage phase. Four uncertain hydraulic parameters (saturated hydraulic conductivity K_S, residual water content θ_r and fitting Mualem-van Genuchten parameters α and n) and two geophysical parameters (Archies's saturation exponent n_a and voltage coupling coefficient at saturation C_{sat}) are investigated. GSA of SP signals is performed by computing the variance-based sensitivity indices using Polynomial Chaos Expansion (PCE). To reduce the number of PCE coefficients while maintaining high PCE orders, we use the efficient sparse PCE algorithm developed by Shao et al. (2017) which selects the best sparse PCE from a given data set using the Kashyap Information Criterion (KIC).

In the second part of this study, we investigate the identifiability of hydro-geophysical parameters from SP measurements. To this aim, parameter estimation is performed using two different approaches. The first is a Bayesian approach in which model parameters are treated as random variables and characterized by their probability density functions. With this approach, the prior knowledge about the model and the observed data are merged to define the joint posterior probability distribution function of the parameters. In the sequel, Bayesian

analysis is conducted using the DREAM$_{(ZS)}$ software (Laloy and Vrugt, 2012; Vrugt, 2016) based on the Markov Chain Monte Carlo (MCMC) method. MCMC has been successfully used in various inverse problems (e.g., Vrugt et al., 2003, 2008; Arora et al., 2012; Younes et al., 2017). The MCMC method yields an ensemble of possible parameter sets that satisfactorily fit the available data. These sets are then employed to estimate the posterior parameter distributions and hence the optimal parameter values and the associated 95% Confidence Intervals (CIs) in order to quantify parameter's uncertainty. The second inversion approach is the commonly used First-Order Approximation (FOA) approach based on the standard Levenberg-Marquardt algorithm. Two scenarios are considered to check whether FOA can provide reliable estimation of parameters and associated uncertainties for the investigated highly nonlinear hydrogeophysical problem in the case of abundant data (small uncertainty regions) and in the case of scarcity of data (large uncertainty regions). In the first scenario, SP data collected from sensors at five different locations are taken into account for the calibration. In the second scenario; only the SP data from one sensor are used for model calibration.

The present study is decomposed as follows. Section 2 presents the hydrogeophysical model and the reference solution. Section 3 reports on the GSA results of SP signals. Then, Section 4 discusses results of parameter estimation with both MCMC and FOA approaches for the two investigated scenarios.

2. Test case description and numerical solution

2.1. Test case description

The test case considered in this work is similar to the laboratory experiment developed in Mboh et al. (2012) involving a falling-head infiltration phase followed by a drainage phase (Figure 1). This experiment is representative of several laboratory SP experiments (Linde et

al., 2007; Allegre et al., 2010; Jougnot and Linde, 2013, among others). Quartz sand is evenly packed in a plastic tube with an internal diameter of 5 cm to a height of L_s =117.5 cm. The column is initially saturated with a ponding of L_w =48 cm above the soil surface. Five sensors allowing SP measurements are installed at respectively 5, 29, 53, 77, and 101 cm from the surface. The column has a zero pressure head maintained at its bottom. At the top of the column, the boundary condition corresponds to a Dirichlet condition with a prescribed pressure head condition during the falling-head phase followed by a Neumann condition with zero infiltration flux during the drainage phase. During the falling-head phase, the prescribed pressure head h_{top} has an exponential behavior driven by the saturated conductivity $h_{top} = \left(L_s + L_w\right) e^{-\frac{K_s}{L_s} t} - L_s$. The falling-head phase remains until the ponding vanishes at the critical time $t_c = -\frac{L_s}{K_s} \ln\left(\frac{L_s}{L_s + L_w}\right)$.

2.2. Mathematical model

The total electrical current density $\boldsymbol{j}$ [A m^{-2}] is determined from the generalized Ohm's law as follows:

$$\boldsymbol{j} = -\sigma \nabla \varphi + \boldsymbol{j}_s \tag{1}$$

where φ [V] is the streaming potential, $\boldsymbol{j}_s$ [A m^{-2}] is the streaming current density and σ [S m^{-1}] is the electrical conductivity distribution assumed isotropic.

Hence, the conservation equation ($\nabla . \boldsymbol{j} = 0$) writes

$$\nabla . \left(\sigma \nabla \varphi\right) = \nabla . \boldsymbol{j}_s \tag{2}$$

Besides, the electrical conductivity distribution can be estimated using the saturation $S_w = \theta / \theta_s$ as follows (Mboh et al., 2012)

$$\sigma = \sigma_{sat} S_w^{\,n_a} \tag{3}$$

where σ_{sat} is the electric conductivity at saturation [S m^{-1}] and n_a is the Archies's saturation exponent (Archie, 1942).

The streaming current density $\boldsymbol{j}_s$ can be related to the Darcy velocity $\boldsymbol{q}$ [cm min^{-1}] by (Linde et al., 2007 ; Revil et al., 2007)

$$\boldsymbol{j}_s = \left(-\sigma_{sat} \frac{\rho g}{K_s} C_{sat} S_w \right) \boldsymbol{q} \tag{4}$$

where K_s is the saturated hydraulic conductivity [cm min^{-1}], ρ is the water density [kg m^{-3}], g is the gravitational acceleration [m s^{-2}] and C_{sat} is the voltage coupling coefficient at saturation [V Pa^{-1}].

Hence, the combination of the previous equations (1-4) leads to the following partial differential equation governing the SP signals:

$$\nabla.\left({S_w}^{n_a} \nabla \varphi \right) = \nabla.\left(-\frac{\rho g C_{sat} S_w}{K_s} \boldsymbol{q} \right) \tag{5}$$

On the other hand, the flow through an unsaturated soil column can be modelled by the one-dimensional Richard's equation:

$$\frac{\partial \theta}{\partial t} = \left(c(h) + S_s \frac{\theta}{\theta_s} \right) \frac{\partial H}{\partial t} = -\nabla.\boldsymbol{q} \tag{6}$$

where H [cm] and h [cm] are respectively the hydraulic and pressure head such as $H = h - z$; z [cm] is the depth (downward positive); S_s (-) is the specific storage; θ_s [cm^3.cm^{-3}] and θ are the saturated and actual water contents, respectively; $c(h)$ [cm^{-1}] is the specific moisture capacity; and $K(h)$ [cm min^{-1}] is the hydraulic conductivity.

The water velocity $\boldsymbol{q}$ is given from the Darcy's law:

$$\boldsymbol{q} = -K(h) \nabla H \tag{6}$$

In the current study, the standard models of Mualem (1976) and Van Genuchten (1980) are used to relate pressure head, hydraulic conductivity and water content,

$$S_e(h) = \frac{\theta(h) - \theta_r}{\theta_s - \theta_r} = \begin{cases} \dfrac{1}{\left(1 + |\alpha h|^n\right)^m} & h < 0 \\ 1 & h \geq 0 \end{cases}$$
$$K(S_e) = K_s S_e^{1/2} \left[1 - \left(1 - S_e^{1/m}\right)^m\right]^2 \quad (7)$$

where S_e (-) is the effective saturation, θ_r [cm^3 cm $^{-3}$] is the residual water content, K_s [cm.min^{-1}] is the saturated hydraulic conductivity, $m = 1 - 1/n$, α [cm^{-1}] and n [-] are the Mualem van-Genuchten shape parameters.

2.3. Numerical model

Although, several numerical techniques have been developed to for the solution of the multidimensional Richards equation (e.g., Fahs et al., 2009; Belfort et al., 2009, Younes et al., 2013; Deng and Wang, 2017), the standard finite volume method is used here for the spatial discretization of the one dimensional Richard's equation (6). The integration of this equation over the finite volume *i* between *i-1/2* and *i+1/2* gives

$$\int_{i-1/2}^{i+1/2} \left(c(h) + S_s \frac{\theta}{\theta_s} \right) \frac{\partial H}{\partial t} dz = q_{i-1/2} - q_{i+1/2} \quad (8)$$

using expressions of the Darcy velocity at the element interfaces $q_{i-1/2} = -\dfrac{K_{i-1/2}}{\Delta z}\left(H_i - H_{i-1}\right)$ and $q_{i+1/2} = -\dfrac{K_{i+1/2}}{\Delta z}\left(H_{i+1} - H_i\right)$ in the case of a uniform spatial discretization with a spatial step Δz, we obtain,

$$\Delta z \left(c_i + S_s \frac{\theta_i}{\theta_s} \right) \frac{\partial H_i}{\partial t} = K_{i+1/2}\left(H_{i+1} - H_i\right) - K_{i-1/2}\left(H_i - H_{i-1}\right) \quad (9)$$

Using $\tau = S_w^{n_a}$ and $\delta = \frac{\rho g C_{sat} S_w}{K_s}$, the integration of the equation (5) over the finite volume *i* yields

$$\frac{\tau_{i+1/2}}{\Delta z}\left(\varphi_{i+1}-\varphi_i\right)-\frac{\tau_{i-1/2}}{\Delta z}\left(\varphi_i-\varphi_{i-1}\right)-\delta_{i+1/2}K_{i+1/2}\left(H_{i+1}-H_i\right)+\delta_{i-1/2}K_{i-1/2}\left(H_i-H_{i-1}\right)=0 \quad (10)$$

where the values at the interface $\tau_{i\pm1/2}$, $\delta_{i\pm1/2}$ and $K_{i\pm1/2}$ are calculated using the arithmetic mean between adjacent elements (for instance, $\tau_{i+1/2} = \frac{\tau_i + \tau_{i+1}}{2}$).

Then, the temporal discretization of the obtained nonlinear ODE/DAE system (9-10) is performed with the method of lines (MOL) using the DASPK (Brown et al., 1994) time solver. The MOL is suitable for strongly nonlinear systems since it allows high order temporal integration methods with formal error estimation and control (Miller et al., 1998; Younes et al., 2009; Fahs et al., 2009, 2011). In the current study, the relative and absolute local error tolerances are fixed to 10^{-6}.

Numerical simulations are performed assuming typical MVG hydraulic parameters for the sandy soil with (according to Carsel and Parrish, 1988) $K_s = 0.495$ cm/min, $\theta_s = 0.43$ cm^3/cm^3, $\theta_r = 0.045\,cm^3/cm^3$, $\alpha = 0.145\,cm^{-1}$ and $n = 2.68$. The voltage coupling coefficient at saturation is $C_{sat} = -2.9 10^{-7}$ V/Pa and the Archies's saturation exponent is $n_a = 1.6$.

Based on these hydraulic and geophysical parameters, a reference (mesh independent) solution is obtained using a uniform mesh of 235 cells of 0.5 cm length. Data are generated by sampling the output SP signals every 10 min during 1800 min. Figure 2 shows that the SP signals have an almost linear behavior in the saturated falling-head phase. During the drainage phase, they have a nonlinear behavior and approach the zero voltage for the dry conditions occurring toward the end of the experiment. The SP signals are noised with independent Gaussian random noises with a standard deviation of 2.73 10^{-5} V. This noise level was

obtained by Mboh et al. (2012) from laboratory measurements. The noised data (Figure 2) are used as "observations" in the calibration exercise.

3. Global sensitivity analysis of SP signals

3.1. GSA method

The aim of GSA is to assess the effect of the variation of parameters on the model output (Mara and Tarantola, 2008). Such knowledge is important for determining the most influential parameters as well as their regions and periods of influence (Fajraoui et al., 2011). The sensitivity of a model to its parameters can be assessed using Variance-based sensitivity indices. These indices evaluate the contribution of each parameter to the variance of the model (Sobol', 2001). The polynomial chaos theory (Wiener, 1938), has been largely used to perform variance-based sensitivity analysis of computer models (see for instance, Sudret, 2008; Blatman and Sudret, 2010; Fajraoui et al., 2012; Younes et al., 2016; Shao et al., 2017; Mara et al., 2017). It can be stated that the PCE method is a surrogate-based approach. However, we argue that this method employs ANOVA (Analysis Of Variance) decomposition and hence can be considered as a spectral method (such as the Fourier amplitude sensitivity test, Cukier et al., 1973; Saltelli et al., 1999). Indeed, with this method, the sensitivity indices are directly obtained from the PCE coefficients without needing to run the surrogate model.

Let us consider a mathematical model with a random response $f(\boldsymbol{\xi})$ which depends on d independent random parameters $\boldsymbol{\xi} = \{\xi_1, \xi_2, ..., \xi_d\}$. With PCE, $f(\boldsymbol{\xi})$ is expanded using a set of orthonormal multivariate polynomials (up to a polynomial degree *p*):

$$f(\boldsymbol{\xi}) \approx \sum_{|\alpha| \leq p} s_\alpha \Psi_\alpha(\boldsymbol{\xi}) \tag{8}$$

where $\alpha = \alpha_1 ... \alpha_d \in \mathbb{N}^d$ is a d^{th}-dimensional index. The s_α's are the polynomial coefficients and Ψ_α's are the generalized polynomial chaos of degree $|\alpha| = \sum_{i=1}^{d} \alpha_i$, such as Hermite, Legendre and Jacobi polynomials, for instance. In this work, Legendre polynomials are employed because uniform distributions are considered for the parameters. The non-informative uniform distributions are used here to express the absence of prior information which makes all possible values of the parameter equally likely.

Equation (8) is similar to an ANOVA representation of the original model (Sobol' 1993), from which it is straightforward to express $V[f(\xi)]$, the variance of $f(\xi)$ as the sum of the partial contribution of the inputs,

$$V[f(\xi)] = \sum_{\alpha} s_\alpha^2 , \tag{9}$$

The first-order sensitivity index S_i and the total sensitivity index ST_i are defined by

$$S_i = \frac{V[E[f(\xi)|\xi_i]]}{V[f(\xi)]} \in [0,1], \tag{10}$$

$$ST_i = \frac{E[V[f(\xi)|\xi_{\sim i}]]}{V[f(\xi)]} \in [0,1], \tag{11}$$

where $\xi_{\sim i} = \xi \setminus \xi_i$, $E[\,|\,]$ is the conditional expectation operator and $V[\,|\,]$ the conditional variance. S_i measures the amount of variance of $f(\xi)$ due to ξ_i alone, while $ST_i \geq S_i$ measures the amount of all contributions of ξ_i to the variance of $f(\xi)$, including its cooperative non-linear contributions with the other parameters ξ_j. The input/output relationship is said *additive* when $ST_i = S_i, \forall i = 1,..,d$, and in this case $\sum_{i=1}^{d} S_i = 1$.

In the sequel, a PCE is constructed for each SP signal at each observable time. The number of coefficients for a full PCE representation is $P = (d+p)!/(d!\,p!)$. The evaluation of the PCE

coefficients requires at least P simulations of the nonlinear hydrogeophysical model. Note that P increases quickly with the order of the PCE and the number of parameters. Hence, several sparse PCE representations, where only the significant coefficients are sought, have been proposed in the literature in order to reduce the computational cost of the estimation of the Sobol indices. For instance, Blatman and Sudret (2010) developed a sparse PCE representation using an iterative forward-backward approach based on non-intrusive regression. Fajraoui et al., (2012) developed a technique where only the sensitive coefficients (that affect significantly model variance) are retained in the PCE. Recently, Shao et al., (2017), developed an algorithm based on Bayesian Model Averaging (BMA) to select the best sparse PCE from a given data set using the Kashyap Information Criterion (KIC) (Kayshap, 1982). The main idea of this algorithm is to increase progressively the degree of an initial PCE and compute the KIC until obtaining a satisfactory representation of model responses. This algorithm is used hereafter to compute the sensitivity indices of the SP signals.

3.2. GSA results

The SP responses are considered for uniformly distributed parameters over the large intervals shown in Table1. These intervals include the reference values reported in Mboh et al. (2012). The sensitivity indices of the six input parameters $(K_s, \theta_r, \alpha, n, n_a, C_{sat})$ are estimated using an experimental design formed by $N = 2^{12} = 4096$ parameter sets. The order of the sparse PCE is automatically adapted for each observable time and location. For some observable times, the PCE is highly sparse; it reaches a degree of 31 but contains only 112 nonzero coefficients.

Figure 3 depicts the temporal distribution of the streaming potential variance, represented by the blue curve, and the relative contribution of the parameters, represented by the shaded area. This figure corresponds to the temporal ANOVA decomposition for the sensor 1 (at 5 cm

267 from the soil surface) and for the sensor 4 (at 77 cm from the soil surface). Interactions
268 between parameters are represented by the blank region between the variance curves and the
269 shaded area. Note that because Dirichlet boundary condition with zero SP is maintained at the
270 outlet boundary, the variance of the SP signal is zero at the bottom and reaches its maximum
271 value near the soil surface. Hence, the variance is higher for the first sensor, located at 5 cm
272 from the soil surface (Figure 3a) than for the sensor 4 located at 77 cm (Figure 3b).
273 The SP signals at different altitudes exhibit similar behavior (Figure 3). In the following, we
274 comment on the results of sensor 1 (Figure 3a). Because K_s varies between 0.1 cm min^{-1} and
275 2 cm min^{-1}, the saturated falling-head phase remains until the ponding vanishes at
276 $t_c = -\frac{L_s}{K_s}\ln\left(\frac{L_s}{L_s + L_w}\right)$. Depending on the value of K_s (see Table 1), t_c varies between $t_1 = 20$
277 min and $t_2 = 403$ min. Thus, in Figure 3a, we can see that during a first time period $(t \le t_1)$,
278 the SP signal is strongly influenced by the value of the parameter C_{sat}. The first order and
279 total sensitivity indices at $t = 10$ min (Table 2a) confirm that only the saturated parameters K_s
280 and C_{sat} are influential. C_{sat} is about 17 times more influential than K_s. As expected, the
281 remaining parameters have no influence during the first period. The total variance is 0.72 mv
282 and there is no interaction between the two parameters K_s and C_{sat} since $ST_i = S_i$ for both
283 and $\sum_{i=1}^{d} S_i = 1$.
284 During the second period $(t_1 \le t \le t_2)$, the flow is either saturated or unsaturated depending on
285 the value of K_s. Figure 3a shows that the variance of the SP signal exhibits its maximum
286 value around 2.4 mv with strong influences of the parameters K_s and C_{sat} and weak
287 interactions between them (small blank region between the variance curve and the shaded
288 area). These results are confirmed by the sensitivity indices calculated at $t = 70$ min and

289 reported in Table 2a for the sensor 1. Both first order and total sensitivity indices indicate that
290 K_s is the most influential parameter. The second influential parameter is C_{sat} which has a
291 total sensitivity index about 12 times less than K_s. The parameter α is irrelevant since its
292 total sensitivity index is 109 times less than K_s and its partial variance is
293 $V_i = S_i \times V_T = 0.01mv$ which is less than the 95% confidence interval associated to the SP
294 measurement ($\pm 0.055mv$). The total variance at $t = 70$ min is calculated to be $2.17\,mv$ and
295 the output/input relationship is close to be additive since $\sum_{i=1}^{d} S_i = 0.94$ which means that
296 interactions between parameters exist but are not significant.
297 During the third period $(t \geq t_2)$, the variance of the SP signal reduces to 0.3 mv (Figure 3a)
298 and significant interactions are observed between parameters (large blank region between the
299 shaded area and the variance curve). Table 2a shows that for $t = 800$ min, which corresponds
300 to dry conditions, the total variance is 0.22. First-order sensitivity indices are very small,
301 except for θ_r. The latter is highly influential since it has a significant first-order sensitivity
302 index ($S_i = 0.27$) and a more significant total- sensitivity index ($ST_i = 0.74$). The parameters
303 C_{sat} and K_s are irrelevant, they have very small first-order and total sensitivity indices.
304 Further, strong interactions are observed between the parameters since the sum of the first-
305 order indices is far from 1 ($\sum_{i=1}^{d} S_i = 0.47$). The total sensitivity indices are significantly
306 different from first-order sensitivity indices for almost all parameters. For instance, the ratio
307 between these two indices is around 4 for α, 5 for n_a and 7 for n. The total sensitivity index
308 of α remains small (0.065), whereas, significant total sensitivity indices are obtained for n (
309 $ST_i = 0.27$) and n_a ($ST_i = 0.47$) which indicates that these two parameters are influential

(although their first order sensitivity indices are small) because of interaction between parameters.

Figure 3b shows similar behavior for the sensor 4 located at 77 cm from the soil surface. The results in Table 2b indicate that the total variance observed at t = 10, 70 and 800 min are around 8 times less than for the sensor 1. For the first time period, the first and total sensitivity indices are identical to those observed for the sensor 1 since saturated conditions occur inside the whole column and the same effect of K_s and C_{sat} can be observed whatever the location inside the column. For the second time period, the sensitivity indices for sensor 4 (Table 2b) are similar to those observed for the sensor 1. However, the results for the third time period show an improvement of the relevance of the parameter α with an increase of both first and total sensitivity indices. Indeed, compared to the results of the sensor1, both first order and total sensitivity indices have tripled. Moreover, the total sensitivity index for α ($ST_i = 0.22$) becomes close to that of n ($ST_i = 0.24$).

In summary, the GSA applied to SP signals identifies the influential parameters and their periods of influence and shows that

- the parameter C_{sat} is highly influential during the first time period $(t \le t_1)$ where no interactions are observed between parameters;
- the parameter K_s is highly influential during the second time period $(t_1 \le t \le t_2)$ where small interactions occur between parameters;
- the parameters θ_r, n and n_a are influential during the third time period $(t \ge t_2)$ where dry conditions occur. During this period, strong interactions take place between parameters;

- the parameter α has no influence on the SP signals during the two first periods and presents a very small influence ($S_i = 0.015$ and $ST_i = 0.065$) during the third period on the sensor 1 (near the surface of the column);
- the relevance of the parameter α improves with the distance from the soil surface, although the total variance diminishes with respect to this distance. The influence of α becomes significant ($ST_i = 0.22$) on the sensor 4 (located at 77 cm from the soil surface) during the third period.

4. Parameter estimation

4.1. MCMC and FOA approaches

Calibration of computer models is an essential task since some parameters (like the Mualem van-Genuchten shape parameters α and n) cannot be directly measured. In such an exercise, the unknown model parameters are investigated by facing the model responses to the observations. Recently, Mboh et al. (2012) showed that inversion of SP signals can yield accurate estimate of the saturated hydraulic conductivity K_S, the MVG fitting parameters α and n and the Archie's saturation exponent (n_a). Moreover, they showed that the quality of the estimation was comparable to that obtained from the calibration of pressure heads. In their study, Mboh et al. (2012) used the FOA approach with the Shuffled Complex Evolution optimization algorithm SCE-UA (Duan et al., 1993).

As important as the determination of the optimal parameter sets are the associated 95% Confidence Intervals (CIs) to quantify uncertainty on the estimated values. The determination of CIs is not straightforward if the observed model responses are highly nonlinear functions of model parameters (Christensen and Cooley, 1999). In the sequel, parameter estimation is performed using two approaches: the popular FOA approach and the Bayesian approach based on the Markov chain Monte Carlo (MCMC) sampler. Contrarily to FOA, the MCMC

356 method is robust since no assumptions of model linearity or differentiability are required.
357 Furthermore, prior information available for the parameters can be included. MCMC provides
358 not only an optimal point estimate of the parameters but also a quantification of the entire
359 parameter space. Several MCMC strategies have been developed for Bayesian sampling of
360 the parameter space (Gallagher and Doherty, 2007; Vrugt, 2016). In groundwater and vadose
361 zone modeling context, the most widely used of these strategies is the Metropolis Hastings
362 algorithm (Metropolis et al., 1953; Hastings, 1970). It proceeds as follows (Gelman et al.,
363 1996):

364 i. Choose an initial candidate $\boldsymbol{x}^0 = \left(\boldsymbol{\xi}^0, \sigma^0\right)$ formed by the initial estimate of the
365 parameter set $\boldsymbol{\xi}^0$ and the hyperparameter σ^0 and a proposal distribution q that
366 depends on the previous accepted candidate.

367 ii. A new candidate $\boldsymbol{x}^i = \left(\boldsymbol{\xi}^i, \sigma^i\right)$ is generated from the current one $\boldsymbol{x}^{i-1}$ with the
368 generator $q\left(\boldsymbol{x}^i \middle| \boldsymbol{x}^{i-1}\right)$ associated with the transition probability $p\left(\boldsymbol{\xi}^i \middle| \boldsymbol{y}_{mes}, \sigma\right)$.

369 iii. Calculate $p\left(\boldsymbol{\xi}^i \middle| \boldsymbol{y}_{mes}, \sigma\right)$ and compute the ratio $\alpha = \dfrac{p\left(\boldsymbol{\xi}^i \middle| \boldsymbol{y}_{mes}, \sigma\right) q\left(\boldsymbol{x}^i \middle| \boldsymbol{x}^{i-1}\right)}{p\left(\boldsymbol{\xi}^{i-1} \middle| \boldsymbol{y}_{mes}, \sigma\right) q\left(\boldsymbol{x}^{i-1} \middle| \boldsymbol{x}^i\right)}$.
370 Additionally, draw a random number $u \in [0,1]$ from a uniform distribution.

371 iv. If $\alpha \geq u$, then accept the new candidate, otherwise it is rejected.

372 v. Resume from (ii) until the chain $\left\{\boldsymbol{x}^0, ..., \boldsymbol{x}^k\right\}$ converges or a prescribed number of
373 iterations $i_{\max}$ is reached.

374 Many improvements have been proposed in the literature to accelerate the MCMC
375 convergence rate (e.g., Haario et al., 2006; ter Braak and Vrugt, 2008; Dostert et al., 2009,
376 among others). Vrugt et al. (2009a, 2009b) developed the DREAM MCMC sampler based on
377 the differential evolution–Markov Chain method of ter Braak (2006) to improve sampling

efficiency. DREAM runs multiple Markov chains in parallel and uses subspace sampling and outlier chain correction to speed up MCMC convergence (Vrugt, 2016). Laloy and Vrugt (2012) developed the DREAM$_{(ZS)}$ MCMC sampler in which a candidate for each chain is drawn from an archive of past states denoted Z which plays the role of the generator q. The interested readers are referred to Vrugt (2016) for more details about properties and implementation of DREAM and DREAM$_{(ZS)}$. In the current study, the DREAM$_{(ZS)}$ software is used for the MCMC estimation of the hydrogeophysical parameters. Note that because of the large number of model evaluations required, the MCMC method remains rarely used in practical applications compared to the FOA approach. Indeed, with FOA, the CIs are estimated once by assuming that the Jacobian remains constant within the CIs. This assumption was found to be reasonably accurate in nonlinear problems by Donaldson and Scnabel (1987). However, recently, several authors stated that parameter interdependences and model nonlinearities violate this assumption (see for instance, Vrugt and Bouten, 2002; Vurgin et al. 2007; Gallagher and Doherty, 2007; Mertens et al., 2009; Kahl et al., 2015).

In the following, both MCMC and FOA approaches are employed for the inversion of the highly nonlinear hydrogeophysical problem using SP measurements.

4.2. Parameter estimation results

Hydrogeophysical parameters are estimated using the DREAM$_{(ZS)}$ MCMC sampler (Laloy and Vrugt, 2012). Independent uniform distributions are considered for model parameter priors and likelihood hyperparameters (see Table 1). The parameter posterior distribution writes:

$$p\left(\boldsymbol{\xi} \mid \boldsymbol{y}_{mes}, \sigma\right) \propto \sigma^{-N} \exp\left(-\frac{SS\left(\boldsymbol{\xi}\right)}{2\sigma^2}\right) \tag{9}$$

where $SS(\xi) = \sum_{k=1}^{N} \left(y_{mes}^{(k)} - y_{mod}^{(k)}(\xi) \right)^2$ is the sum of the squared differences between the observed $y_{mes}^{(k)}$ and modeled $y_{mod}^{(k)}$ SP signals at time t_k for N total number of SP observations.

The DREAM$_{(ZS)}$ software computes multiple sub-chains in parallel to thoroughly explore the parameter space. Taking the last 25% of individuals (when the chains have converged) yields multiple sets used to estimate the updated parameter distributions and therefore the optimal parameter values and their CIs. In the sequel, the DREAM$_{(ZS)}$ MCMC sampler is used with 3 parallel chains.

We assume that the saturated water content has been initially measured with a fair degree of accuracy. However, instead of fixing its value (as in Kool et al. (1987), van Dam et al. (1994), Nützmann et al., (1998) among others), we assign to θ_s a Gaussian distribution to take into account associated uncertainty and its effect on the estimation of the rest of parameters. It is assumed here that the saturated water content was accurately measured to be $\theta_s = 0.43$ cm3.cm^{-3} by weighing the saturated soil. The corresponding error measurements are independently and normally distributed with a zero mean and a standard deviation $\sigma_\theta = 0.01$ cm3.cm^{-3}. Hence a Gaussian distribution is assigned to θ_s with a mean value of 0.43 cm^3.cm^{-3} and a 95% CI $[0.41 - 0.45]$ cm^3.cm^{-3}. The rest of hydrogeophysical parameters have non informative uniform distributions over the ranges reported in Table 1. The error (measurement) variance is also considered unknown and is simultaneously estimated with the physical parameters. Two scenarios are considered to check whether the FOA approach can provide reliable estimation of parameters and associated uncertainties for the investigated highly nonlinear hydrogeophysical problem both in the case of abundant data (small uncertainty regions) and in the case of scarcity of data (large uncertainty regions). In the first scenario, SP data collected from the sensors located at the five locations are taken into

account for the calibration. In the second scenario; only the SP data from the first sensor located at 5 cm from the soil surface serve as conditioning information for model calibration. Results of the MCMC sampler are compared to those of FOA approach for both scenarios.

Scenario 1: Inversion using all SP measurements

The Figure 4 shows the results obtained with MCMC when the SP data of the five sensors are used for the calibration. The "on-diagonal" plots in this figure display the posterior parameter distributions, whereas the "off-diagonal" plots represent the correlations between parameters in the MCMC sample. Figure 4 shows nearly bell-shaped posterior distributions for all parameters. A strong correlation is observed between θ_r and n_a ($r = 0.98$).

From the obtained MCMC sample, it is straightforward to estimate the posterior 95% confidence interval of each parameter. The latter as well as the mean estimate value of each parameter obtained with both MCMC and FOA approaches are reported in Table 3.

The results this table show that the parameters are well estimated from the SP measurements since (*i*) identified mean values are very close to the reference solution, (*ii*) all confidence intervals include the reference solution and (*iii*) the confidence intervals are rather narrow. The saturated parameters K_S and C_{sat} are very well estimated (with CIs around 2%) because of data collected during the falling-head phase where only these two parameters are influential.

The posterior CI of the parameter θ_s is similar to its prior CI. The parameter α is reasonably well estimated with a CI around 35%. Recall that this parameter had very small first-order and total sensitivity indices for sensor 1 but had more significant sensitivity indices for the sensors away from the soil surface (see results for sensor 4 in Table 2b). The parameter θ_r is estimated with a CI around 90% although it was highly influential for all sensors (for instance, a first-order sensitivity index of 0.27 and a total order of 0.74 for sensor 1). The

parameters n and n_a had similar GSA behavior with small first-order sensitivities (respectively 0.038 and 0.094 for sensor 1) and large total sensitivities (respectively 0.266 and 0.4715 for sensor 1), however, the inversion shows that the parameter n is well estimated with a CI less than 10% whereas the parameter n_a is less well estimated with a CI around 35%. These results suggest that GSA outcomes should be interpreted with caution in the context of parameter estimation since (*i*) a parameter which is not relevant for the model output in one sensor can be influential for another sensor and (*ii*) GSA does not presume on the quality of the estimation since two parameters with similar sensitivity indices can have different quality of estimation by the inversion procedure.

Further, the results of Table 3 show that FOA and MCMC approaches yield similar mean estimated values. Moreover, very good agreement is observed between FOA and MCMC uncertainty bounds. Concerning the efficiency of the two calibration methods for this scenario, the FOA approach is by far the most efficient method since it requires only 95s of CPU time. The MCMC method was terminated after 16,000 model runs which required 14,116s. The convergence was reached at around 12,000 model runs. The last 4,000 runs were used to estimate the statistical measures of the posterior distribution. Recall that that contrarily to FOA, MCMC can include prior information available for the parameters and allows a quantification of the entire parameter space.

Scenario 2: Inversion using only SP measurements near the surface

In this scenario, the number of measurements used for the calibration is strongly reduced. Only SP measurements from sensor 1 (located at 5 cm blow de soil surface) are considered.

The results of MCMC are plotted in the Figure 5. The correlation observed between θ_r and n_a decreases slightly to $r = 0.95$. Almost bell-shaped posterior distributions are observed for all parameters except for the parameters θ_r and α.

The results obtained with MCMC and FOA approaches depicted in Table 4 show that

- The FOA approach yields accurate mean estimated values similar to MCMC results for all parameters;
- The MCMC and FOA mean estimated values are close to the reference solution and to the previous scenario. The maximum difference is observed for θ_r for which the mean estimated value with scenario 2 is 15% greater than for scenario 1
- The MCMC CIs for the parameters K_S, θ_s, n and C_{sat} are close to the previous scenario. The parameters θ_s and n are well estimated (CIs < 10%) and the parameters K_S and C_{sat} are very well estimated (CIs $\leq$ 5%).
- Due to the reduction of the number of data used for model calibration in the scenario 2, the MCMC CIs for the parameters n_a, α and θ_r are much larger than in the previous scenario. Indeed, compared to scenario1, the CI for n_a and θ_r increases by around 60% whereas the CI of α is 3 times larger than for the scenario 1.
- The FOA method yields accurate CIs for the parameters θ_s, n, n_a and C_{sat} whereas it overestimates the CIs of θ_r (by 24%), K_S (by 100%) and α (by 427%). Unphysical uncertainty region (including negative values) is obtained for the parameter α

These results show that the FOA can fail to provide realistic parameter uncertainties and can yield larger CIs than their corresponding nonlinear MCMC counterpart. Indeed, the linearization in the FOA method assumes that the Jacobian remains constant across the CIs. This assumption was quite fulfilled for the first scenario in which a large number of

494 measurements insured small uncertainty regions. However, the assumption is not fulfilled for
495 some parameters of the current scenario because of the large uncertainty regions induced by
496 the reduction of the number of SP measurements.
497 Concerning the efficiency of the calibration methods, the FOA required approximately 174s
498 of CPU time, the MCMC required much more runs to reach the convergence than in the
499 previous scenario. Indeed, the sampler was used with 50,000 runs (35,000 runs were
500 necessary to reach the convergence).

501 ## 4. Conclusions

502 In this work, a synthetic test case dealing with SP signals during drainage experiment has
503 been studied. The test case is similar to the laboratory experiment developed in Mboh et al.
504 (2012) involving a falling-head infiltration phase followed by a drainage phase. GSA and
505 Bayesian parameter inference have been applied to investigate (*i*) the influence of hydraulic
506 and geophysical parameters on the SP signals and (*ii*) the identifiability of hydro-geophysical
507 parameters using only SP measurements. The GSA was performed using variance-based
508 sensitivity indices which allow measuring the contribution of each parameter (alone or by
509 interaction with other parameters) to the output variance. The sensitivity indices have been
510 calculated using a PCE representation of the SP signals. To reduce the number of coefficients
511 and explore PCE with high orders, we used the efficient sparse PCE algorithm developed by
512 Shao et al. (2017) which selects the best sparse PCE from a given data set using the Kashyap
513 Information Criterion (KIC).
514 The GSA applied to SP signals showed that the parameters C_{sat} and K_s are highly influential
515 during the first period corresponding to saturated conditions. The parameters θ_r, n and n_a
516 are influential when dry conditions occur. In such conditions, strong interactions take place
517 between these parameters. The parameter α has a very small influence on the SP signals near

518 the soil surface but its sensitivity increases with depth although the total variance decreases
519 with depth.
520 Parameter estimation has been performed using MCMC and FOA approaches to check
521 whether FOA can provide reliable estimation of parameters and associated uncertainties for
522 the investigated highly nonlinear hydrogeophysical problem. All hydraulic (K_S, θ_r, α and
523 n) and geophysical (n_a and C_{sat}) parameters can be reasonably estimated in the first scenario
524 when the whole SP data (measured at five different locations) are used as conditioning
525 information for the model calibration. The confrontation with GSA results shows that the
526 latter should be interpreted with caution when used in the context of parameter estimation
527 since (*i*) a parameter which is not relevant for the model output in one sensor can be
528 influential for another sensor and (*ii*) GSA does not presume on the quality of the estimation
529 since two parameters with similar sensitivity indices can have different quality of estimation
530 by the inverse procedure (see for instance, parameters n and n_a). Furthermore, although the
531 studied problem is highly nonlinear, the FOA approach provides accurate estimations of both
532 mean parameter values and CIs in the first scenario. These results are identical to those
533 obtained with MCMC.
534 When the number of SP measurements used for the calibration is considerably reduced
535 (scarcity of data), the MCMC inversion provides larger parameters' uncertainty regions. The
536 FOA approach yields accurate mean parameter values (in agreement with MCMC results) but
537 inaccurate and even unphysical CIs for some parameters with large uncertainty regions.
538

References

Allègre, V., Jouniaux, L., Lehmann, F. and Sailhac, P.: Streaming potential dependence on water-content in Fontainebleau sand, Geophysical Journal International, 182(3), 1248–1266, doi:10.1111/j.1365-246X.2010.04716.x, 2010.

Archie, G. E.: The Electrical Resistivity Log as an Aid in Determining Some Reservoir Characteristics, Transactions of the AIME, 146(01), 54–62, doi:10.2118/942054-G, 1942.

Arora, B., Mohanty, B. P. and McGuire, J. T.: Uncertainty in dual permeability model parameters for structured soils, Water Resources Research, 48(1), doi:10.1029/2011WR010500, 2012.

Belfort, B., Ramasomanan, F., Younes, A., Lehmann, F.: An efficient Lumped Mixed Hybrid Finite Element Formulation for variably saturated groundwater flow. Vadoze Zone Journal. 8 (2), 352-362, doi: 10.2136/vzj2008.0108, 2009.

Blatman, G. and Sudret, B.: Efficient computation of global sensitivity indices using sparse polynomial chaos expansions, Reliability Engineering & System Safety, 95(11), 1216–1229, doi:10.1016/j.ress.2010.06.015, 2010.

Bolève, A., Revil, A., Janod, F., Mattiuzzo, J.L. and Fry, J.-J.: Preferential fluid flow pathways in embankment dams imaged by self-potential tomography. Near Surf. Geophys. 7:447–462. doi:10.3997/1873-0604.2009012, 2009.

Bogoslovsky, V.A. and Ogilvy, A.A.: Deformation of natural electric fields near drainage structures. Geophys. Prospect. 21:716–723. doi:10.1111/j.1365-2478.1973.tb00053, 1973.

ter Braak, C.J.F.: A Markov Chain Monte Carlo version of the genetic algorithm differential evolution: Easy Bayesian computing for real parameter spaces. Stat Comput. 16:239–249. doi: 10.1007/s11222-006-8769-1, 2006.

ter Braak, C. J. F. and Vrugt, J. A.: Differential Evolution Markov Chain with snooker updater and fewer chains, Statistics and Computing, 18(4), 435–446, doi:10.1007/s11222-008-9104-9, 2008.

Brown, P.N., Hindmarsh, A.C. and Petzold, L.R.: Using Krylov Methods in the Solution of Large-Scale Differential-Algebraic Systems, SIAM J. Sci. Comp., 15, pp. 1467-1488. doi:10.1137/0915088, 1994.

Carsel, R. F. and Parrish, R. S.: Developing joint probability distributions of soil water retention characteristics. Water Resources Research, 24 (5), 755–769,doi: 10.1029/WR024i005p00755,1988.

Christensen, S. and Cooley, R. L.: Evaluation of confidence intervals for a steady-state leaky aquifer model, Advances in Water Resources, 22(8), 807–817, doi:10.1016/S0309-1708(98)00055-4, 1999.

Cukier, R. I., Fortuin, C. M., Shuler, K. E., Petschek, A. G., Schaibly, J. H.: Study of the sensitivity of coupled reaction systems to uncertainties in rate coefficients. I. theory. J. Chemical Physics 59, 3873–3878. 1973.

van Dam, J. C., Stricker, J. N. M. and Droogers, P.: Inverse Method to Determine Soil Hydraulic Functions from Multistep Outflow Experiments, Soil Science Society of America Journal, 58(3), 647, doi:10.2136/sssaj1994.03615995005800030002x, 1994.

Darnet, M., Marquis, G. and Sailhac, P.: Estimating aquifer hydraulic properties from the inversion of surface Streaming Potential (SP) anomalies, Geophysical Research Letters, 30(13), doi:10.1029/2003GL017631, 2003.

Deng, B., Wang, J.: Saturated-unsaturated groundwater modeling using 3D Richards equation with a coordinate transform of nonorthogonal grids. Applied Mathematical Modelling, 50:39–52. doi10.1016/j.apm.2017.05.021; 2017.

Donaldson, J. R. and Schnabel, R. B.: Computational Experience with Confidence Regions and Confidence Intervals for Nonlinear Least Squares, Technometrics, 29(1), 67, doi:10.2307/1269884, 1987.

Dostert, P., Efendiev, Y. and Mohanty, B.: Efficient uncertainty quantification techniques in inverse problems for Richards' equation using coarse-scale simulation models, Advances in Water Resources, 32(3), 329–339, doi:10.1016/j.advwatres.2008.11.009, 2009.

Duan, Q. Y., Gupta, V. K. and Sorooshian, S.: Shuffled complex evolution approach for effective and efficient global minimization, Journal of Optimization Theory and Applications, 76(3), 501–521, doi:10.1007/BF00939380, 1993.

Fahs, M., Younes, A. and Lehmann, F.: An easy and efficient combination of the Mixed Finite Element Method and the Method of Lines for the resolution of Richards' Equation, Environmental Modelling & Software, 24(9), 1122–1126, doi:10.1016/j.envsoft.2009.02.010, 2009.

Fahs, M., Younes, A. and Ackerer, P.: An Efficient Implementation of the Method of Lines for Multicomponent Reactive Transport Equations, Water, Air, & Soil Pollution, 215(1–4), 273–283, doi:10.1007/s11270-010-0477-y, 2011.

Fajraoui, N., Ramasomanana, F., Younes, A., Mara, T. A., Ackerer, P. and Guadagnini, A.: Use of global sensitivity analysis and polynomial chaos expansion for interpretation of nonreactive transport experiments in laboratory-scale porous media, Water Resources Research, 47(2), doi:10.1029/2010WR009639, 2011.

Fajraoui, N., Mara, T. A., Younes, A. and Bouhlila, R.: Reactive Transport Parameter Estimation and Global Sensitivity Analysis Using Sparse Polynomial Chaos Expansion, Water, Air, & Soil Pollution, 223(7), 4183–4197, doi:10.1007/s11270-012-1183-8, 2012.

Fajraoui, N., Fahs, M., Younes, A. and Sudret, B.: Analyzing natural convection in porous enclosure with polynomial chaos expansions: Effect of thermal dispersion, anisotropic permeability and heterogeneity, International Journal of Heat and Mass Transfer, 115, 205–224, doi:10.1016/j.ijheatmasstransfer.2017.07.003, 2017.

Gallagher, M., and Doherty, J.: Parameter estimation and uncertainty analysis for a watershed model, Environmental Modelling & Software, 22(7), 1000–1020, doi:10.1016/j.envsoft.2006.06.007, 2007.

Gelman, A., Carlin, J., Stern, H. Rubin, D.: Bayesian Data Analysis, Second Edition, London, Great Britain: Chapman Hall. 696 p. ISBN: 0-158-48838-8, 1996.

van Genuchten, M. T.: A Closed-form Equation for Predicting the Hydraulic Conductivity of Unsaturated Soils, Soil Science Society of America Journal, 44(5), 892, doi:10.2136/sssaj1980.03615995004400050002x, 1980.

Haario, H., Laine, M., Mira, A. and Saksman, E.: DRAM: Efficient adaptive MCMC, Statistics and Computing, 16(4), 339–354, doi:10.1007/s11222-006-9438-0, 2006.

Hastings, W. K.: Monte Carlo Sampling Methods Using Markov Chains and Their Applications, Biometrika, 57(1), 97, doi:10.2307/2334940, 1970.

Hinnell, A. C., Ferré, T. P. A., Vrugt, J. A., Huisman, J. A., Moysey, S., Rings, J. and Kowalsky, M. B.: Improved extraction of hydrologic information from geophysical data through coupled hydrogeophysical inversion, Water Resources Research, 46(4), doi:10.1029/2008WR007060, 2010.

Ishido, T., and Mizutani, H.: Experimental and theoretical basis of electrokinetic phenomena in rock–water systems and its applications to geophysics. J. Geophys. Res. 86:1763–1775. doi:10.1029/JB086iB03p01763, 1981.

Jardani, A., Revil, A., Bolève, A., Crespy, A., Dupont, J.-P., Barrash, W. and Malama, B.: Tomography of the Darcy velocity from self-potential measurements, Geophysical Research Letters, 34(24), doi:10.1029/2007GL031907, 2007.

Jougnot, D. and Linde, N.: Self-Potentials in Partially Saturated Media: The Importance of Explicit Modeling of Electrode Effects, Vadose Zone Journal, 12(2), 0, doi:10.2136/vzj2012.0169, 2013.

Kahl, G. M., Sidorenko, Y. and Gottesbüren, B.: Local and global inverse modelling strategies to estimate parameters for pesticide leaching from lysimeter studies: Inverse modelling to estimate pesticide leaching parameters from lysimeter studies, Pest Management Science, 71(4), 616–631, doi:10.1002/ps.3914, 2015.

Kayshap, R.L.: Optimal choice of AR and MA parts in autoregressive moving average models, IEEE Trans. Pattern Anal. Machine Intell. 4(2), 99-104, 1982.

Kool, J. B., Parker, J. C. and van Genuchten, M. T.: Parameter estimation for unsaturated flow and transport models — A review, Journal of Hydrology, 91(3–4), 255–293, doi:10.1016/0022-1694(87)90207-1, 1987.

Laloy, E. and Vrugt, J. A.: High-dimensional posterior exploration of hydrologic models using multiple-try DREAM $_{(ZS)}$ and high-performance computing, Water Resources Research, 48(1), doi:10.1029/2011WR010608, 2012.

Linde, N., Jougnot, D., Revil, A., Matthäi, S. K., Arora, T., Renard, D. and Doussan, C.: Streaming current generation in two-phase flow conditions, Geophysical Research Letters, 34(3), doi:10.1029/2006GL028878, 2007.

Mara, T. A. and Tarantola, S.: Application of global sensitivity analysis of model output to

building thermal simulations, Building Simulation, 1(4), 290–302, doi:10.1007/s12273-008-8129-5, 2008.

Mara, T. A., Belfort, B., Fontaine, V. and Younes, A.: Addressing factors fixing setting from given data: A comparison of different methods, Environmental Modelling & Software, 87, 29–38, doi:10.1016/j.envsoft.2016.10.004, 2017.

Mboh, C. M., Huisman, J. A., Zimmermann, E. and Vereecken, H.: Coupled Hydrogeophysical Inversion of Streaming Potential Signals for Unsaturated Soil Hydraulic Properties, Vadose Zone Journal, 11(2), 0, doi:10.2136/vzj2011.0115, 2012.

Mertens, J., Kahl, G., Gottesbüren, B. and Vanderborght, J.: Inverse Modeling of Pesticide Leaching in Lysimeters: Local versus Global and Sequential Single-Objective versus Multiobjective Approaches, Vadose Zone Journal, 8(3), 793, doi:10.2136/vzj2008.0029, 2009.

Metropolis, N., Rosenbluth, A. W., Rosenbluth, M. N., Teller, A. H. and Teller, E.: Equation of State Calculations by Fast Computing Machines, The Journal of Chemical Physics, 21(6), 1087–1092, doi:10.1063/1.1699114, 1953.

Miller, C. T., Williams, G. A., Kelley, C. T. and Tocci, M. D.: Robust solution of Richards' equation for nonuniform porous media, Water Resources Research, 34(10), 2599–2610, doi:10.1029/98WR01673, 1998.

Mualem, Y.: A new model for predicting the hydraulic conductivity of unsaturated porous media, Water Resources Research, 12(3), 513–522, doi:10.1029/WR012i003p00513, 1976.

Nützmann, G., Thiele, M., Maciejewski, S. and Joswig, K.: Inverse modelling techniques for determining hydraulic properties of coarse-textured porous media by transient outflow methods, Advances in Water Resources, 22(3), 273–284, doi:10.1016/S0309-1708(98)00009-8, 1998.

Patella, D.: Introduction to ground surface self-potential tomography. Geophys. Prospect. 45:653–681. doi:10.1046/j.1365-2478.1997.430277, 1997.

Rajabi, M. M., Ataie-Ashtiani, B. and Simmons, C. T.: Polynomial chaos expansions for uncertainty propagation and moment independent sensitivity analysis of seawater intrusion simulations, Journal of Hydrology, 520, 101–122, doi:10.1016/j.jhydrol.2014.11.020, 2015.

Revil, A., Linde, N., Cerepi, A., Jougnot, D., Matthäi, S. and Finsterle, S.: Electrokinetic coupling in unsaturated porous media, Journal of Colloid and Interface Science, 313(1), 315–327, doi:10.1016/j.jcis.2007.03.037, 2007.

Richards, K., Revil, A., Jardani, A., Henderson, F., Batzle, M., and Haas, A.: Pattern of shallow ground water flow at Mount Princeton Hot Springs, Colorado, using geoelectric methods. J. Volcanol. Geotherm. Res. 198:217–232. doi:10.1016/j.jvolgeores.2010.09.001, 2010.

Riva, M., Guadagnini, A. and Dell'Oca, A.: Probabilistic assessment of seawater intrusion under multiple sources of uncertainty, Advances in Water Resources, 75, 93–104, doi:10.1016/j.advwatres.2014.11.002, 2015.

Sailhac, P. and Marquis, G.: Analytic potentials for the forward and inverse modeling of SP anomalies caused by subsurface fluid flow, Geophysical Research Letters, 28(9), 1851–1854, doi:10.1029/2000GL012457, 2001.

Saltelli, A., Tarantola, S. and Chan, K. P.-S.: A Quantitative Model-Independent Method for Global Sensitivity Analysis of Model Output, Technometrics, 41, 39–56, doi:10.1080/00401706.1999.10485594, 1999.

Shao, Q., Younes, A., Fahs, M. and Mara, T. A.: Bayesian sparse polynomial chaos expansion for global sensitivity analysis, Computer Methods in Applied Mechanics and Engineering, 318, 474–496, doi:10.1016/j.cma.2017.01.033, 2017.

Sobol′, I. .: Global sensitivity indices for nonlinear mathematical models and their Monte Carlo estimates, Mathematics and Computers in Simulation, 55(1–3), 271–280, doi:10.1016/S0378-4754(00)00270-6, 2001.

Sobol′, I. M.: Sensitivity estimates for nonlinear mathematical models, Math. Model. Comput. Exp., 407–414, 1993.

Sudret, B.: Global sensitivity analysis using polynomial chaos expansions, Reliability Engineering & System Safety, 93(7), 964–979, doi:10.1016/j.ress.2007.04.002, 2008.

Volkova, E., Iooss, B. and Van Dorpe, F.: Global sensitivity analysis for a numerical model of radionuclide migration from the RRC "Kurchatov Institute" radwaste disposal site, Stochastic Environmental Research and Risk Assessment, 22(1), 17–31, doi:10.1007/s00477-006-0093-y, 2008.

Vrugt, J., Gupta, H. V., Bouten, W. and Sorooshian, S.: A Shuffled Complex Evolution Metropolis algorithm for optimization and uncertainty assessment of hydrologic parameter estimation, Water Resour. Res., 39, 2003.

Vrugt, J. A. and Bouten, W.: Validity of First-Order Approximations to Describe Parameter Uncertainty in Soil Hydrologic Models, Soil Science Society of America Journal, 66(6), 1740, doi:10.2136/sssaj2002.1740, 2002.

Vrugt, J. A., ter Braak, C. J. F., Clark, M. P., Hyman, J. M. and Robinson, B. A.: Treatment of input uncertainty in hydrologic modeling: Doing hydrology backward with Markov chain Monte Carlo simulation: FORCING DATA ERROR USING MCMC SAMPLING, Water Resources Research, 44(12), doi:10.1029/2007WR006720, 2008.

Vrugt, J.A., ter Braak, C.J.F., Diks, C.G.H., Robinson, B.A., Hyman, J.M. and Higdon, D.: Accelerating Markov chain Monte Carlo simulation by differential evolution with self-adaptive randomized subspace sampling. Int. J. Nonlinear Sci. Numer. Simul. 10:273–290. doi:10.1515/IJNSNS.2009.10.3.273. 2009a.

Vrugt, J. A.: Markov chain Monte Carlo simulation using the DREAM software package: Theory, concepts, and MATLAB implementation, Environmental Modelling & Software, 75, 273-316, doi: 10.1016/j.envsoft.2015.08.013, 2016.

Vrugt, J.A., Robinson, B.A., Hyman, J.M.: Self-adaptive multimethod search for global optimization in real parameter spaces. IEEE Trans. Evol. Comput. 13:243–259.

doi:10.1109/TEVC.2008.924428, 2009b.

Vugrin, K. W., Swiler, L. P., Roberts, R. M. , Stucky-Mack, N. J., and Sullivan, S. P.: Confidence region estimation techniques for nonlinear regression in groundwater flow: Three case studies, Water Resour. Res., 43, W03423, doi:10.1029/2005WR004804, 2007.

Wiener, N.: The Homogeneous Chaos, American Journal of Mathematics, 60(4), 897, doi:10.2307/2371268, 1938.

Younes, A., Fahs, M. and Ahmed, S.: Solving density driven flow problems with efficient spatial discretizations and higher-order time integration methods, Advances in Water Resources, 32(3), 340–352, doi:10.1016/j.advwatres.2008.11.003, 2009.

Younes, A., Fahs, M., Belfort, B.: Monotonicity of the cell-centred triangular MPFA method for saturated and unsaturated flow in heterogeneous porous media, Journal of Hydrology, 504, 132-141, doi:10.1016/j.jhydrol.2013.09.041, 2013.

Younes, A., Mara, T. A., Fajraoui, N., Lehmann, F., Belfort, B. and Beydoun, H.: Use of Global Sensitivity Analysis to Help Assess Unsaturated Soil Hydraulic Parameters, Vadose Zone Journal, 12(1), 0, doi:10.2136/vzj2011.0150, 2013.

Younes, A., Delay, F., Fajraoui, N., Fahs, M. and Mara, T. A.: Global sensitivity analysis and Bayesian parameter inference for solute transport in porous media colonized by biofilms, Journal of Contaminant Hydrology, 191, 1–18, doi:10.1016/j.jconhyd.2016.04.007, 2016.

Younes, A., Mara, T., Fahs, M., Grunberger, O. and Ackerer, P.: Hydraulic and transport parameter assessment using column infiltration experiments, Hydrology and Earth System Sciences, 21(5), 2263–2275, doi:10.5194/hess-21-2263-2017, 2017.

Zablocki, C.J.: Streaming potentials resulting from the descent of meteoric water: A possible source mechanism for Kilauean self-potential anomalies. Trans. Geotherm. Resour. Counc. 2:747–748, 1978.

539

List of table captions

Table 1. Reference values, lower and upper bounds for hydraulic and geophysical parameters.

Table 2. The first-order sensitivity index S_i and the total sensitivity index ST_i for the SP signal at 5 cm and 77 cm below the soil surface at different times.

Table 3: Estimated mean values (underlined), confidence intervals (CIs) and size of the posterior CIs (italic) with MCMC and FOA approaches for scenario 1.

Table 4: Estimated mean values (underlined), confidence intervals (CIs) and size of the posterior CIs (italic) with MCMC and FOA approaches for scenario 2.

Parameters	Lower bounds	Upper bounds	Reference values
K_s [cm min^{-1}]	0.1	2	0.495
θ_r [cm^3 min^{-3}]	0	0.2	0.045
α [cm^{-1}]	0.01	0.2	0.145
n	1.5	7	2.68
n_a [-]	1	3	1.6
$C_{sat} \times \left(-10^{-7}\right)$ [V/Pa]	2	4	2.9

Table 1. Reference values, lower and upper bounds for hydraulic and geophysical parameters.

548

	K_s [cm min^{-1}]	θ_r [cm^3 min^{-3}]	α [cm^{-1}]	n	n_a	C_{sat} [V/Pa]
	a- sensor 1 (5 cm from the soil surface)					
	t=10 min (total variance = 0.72)					
S_i	0.055	0	0	0	0	0.942
ST_i	0.057	0	0	0	0	0.945
	t=70 min (total variance = 2.17)					
S_i	0.841	0.217	0.005	0.014	0.008	0.045
ST_i	0.894	0.043	0.008	0.028	0.021	0.078
	t=800 min (total variance = 0.224)					
S_i	0.053	0.266	0.015	0.038	0.094	0.008
ST_i	0.085	0.738	0.065	0.266	0.472	0.041
	b- sensor 4 (77 cm from the soil surface)					
	t=10 min (total variance = 0.094)					
S_i	0.055	0	0	0	0	0.942
ST_i	0.057	0	0	0	0	0.945
	t=70 min (total variance = 0.2744)					
S_i	0.839	0.015	0.014	0.013	0.005	0.053
ST_i	0.891	0.028	0.024	0.025	0.011	0.086
	t=800 min (total variance = 0.224)					
S_i	0.099	0.225	0.054	0.043	0.085	0.01
ST_i	0.138	0.621	0.218	0.238	0.379	0.043

Table 2. The first-order sensitivity index S_i and the total sensitivity index ST_i for the SP signal at 5 cm and 77 cm below the soil surface at different times.

549

	MCMC	FOA
K_S [cm min^{-1}]	**<u>0.49</u>** (0.487-0.498) ***0.01***	**<u>0.49</u>** (0.487-0.497) ***0.01***
θ_s [cm^3 min^{-3}]	**<u>0.43</u>** (0.41-0.45) ***0.04***	**<u>0.43</u>** (0.41-0.45) ***0.04***
θ_r [cm^3 min^{-3}]	**<u>0.046</u>** (0.025-0.068) ***0.04***	**<u>0.046</u>** (0.026-0.066) ***0.04***
α [cm^{-1}]	**<u>0.14</u>** (0.12-0.17) ***0.05***	**<u>0.14</u>** (0.12-0.16) ***0.04***
n	**<u>2.64</u>** (2.54-2.77) ***0.23***	**<u>2.64</u>** (2.54-2.76) ***0.22***
n_a	**<u>1.64</u>** (1.37-1.98) ***0.6***	**<u>1.64</u>** (1.38-1.90) ***0.5***
C_{sat} [V/Pa]	**<u>2.90</u>** (2.89-2.91) ***0.02***	**<u>2.90</u>** (2.89-2.91) ***0.02***

Table 3: Estimated mean values (underlined), confidence intervals (CIs) and size of the posterior CIs (italic) with MCMC and FOA approaches for scenario 1.

550

	MCMC	**FOA**
K_S [cm min^{-1}]	**<u>0.49</u>** (0.481-0.495) ***0.014***	**<u>0.49</u>** (0.474-0.503) ***0.029***
θ_s [cm^3 min^{-3}]	**<u>0.43</u>** (0.41-0.45) ***0.04***	**<u>0.43</u>** (0.41-0.45) ***0.04***
θ_r [cm^3 min^{-3}]	**<u>0.053</u>** (0.011-0.093) ***0.08***	**<u>0.053</u>** (0.002-0.103) ***0.1***
α [cm^{-1}]	**<u>0.13</u>** (0.07-0.20) ***0.13***	**<u>0.13</u>** (-0.15-0.43) ***0.58***
n	**<u>2.54</u>** (2.44-2.68) ***0.24***	**<u>2.56</u>** (2.44-2.68) ***0.24***
n_a	**<u>1.82</u>** (1.36-2.41) ***1.05***	**<u>1.78</u>** (1.29-2.27) ***0.98***
C_{sat} [V/Pa]	**<u>2.89</u>** (2.88-2.91) ***0.03***	**<u>2.89</u>** (2.88-2.91) ***0.03***

Table 4: Estimated mean values (underlined), confidence intervals (CIs) and size of the posterior CIs (italic) with MCMC and FOA approaches for scenario 2.

551

List of figure captions

Figure 1. Illustration of the experimental device.

Figure2. Reference SP signals. Solid lines represent the reference SP solution and dots represent the sets of perturbed data serving as conditioning information for model calibration.

Figure 3. Time distribution of the SP variance at 5cm (a) and 77cm (b) depth. The shaded area under the variance curve represents the partial marginal contributions of the random input parameters; the contribution of interactions between parameters is represented by the blank region between the shaded area and the variance curve.

Figure 4. MCMC solutions when all SP data are considered for the calibration. The diagonal plots represent the inferred posterior probability distribution of the model parameters. The off-diagonal scatterplots represent the pairwise correlations in the MCMC drawing.

Figure 5. MCMC solutions when calibration is performed using only SP data located at 5 cm from the surface. The diagonal plots represent the posterior probability distribution of the parameters. The off-diagonal scatterplots represent the pairwise correlations in the MCMC drawing.

572

573

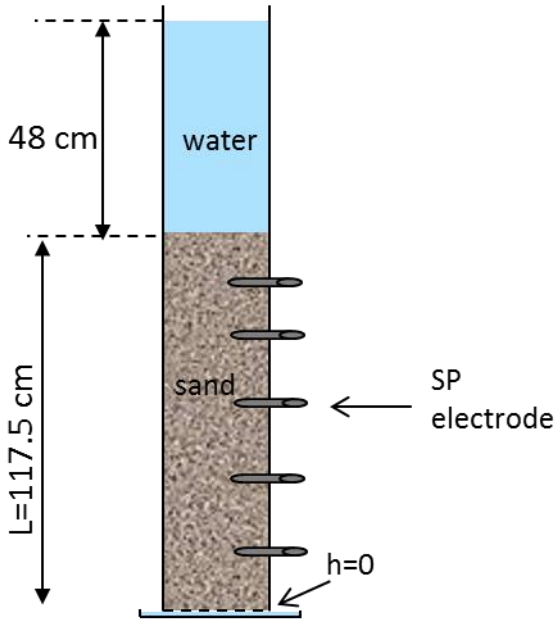

574

575

576 Figure 1. Illustration of the experimental device.

577

578

579

580

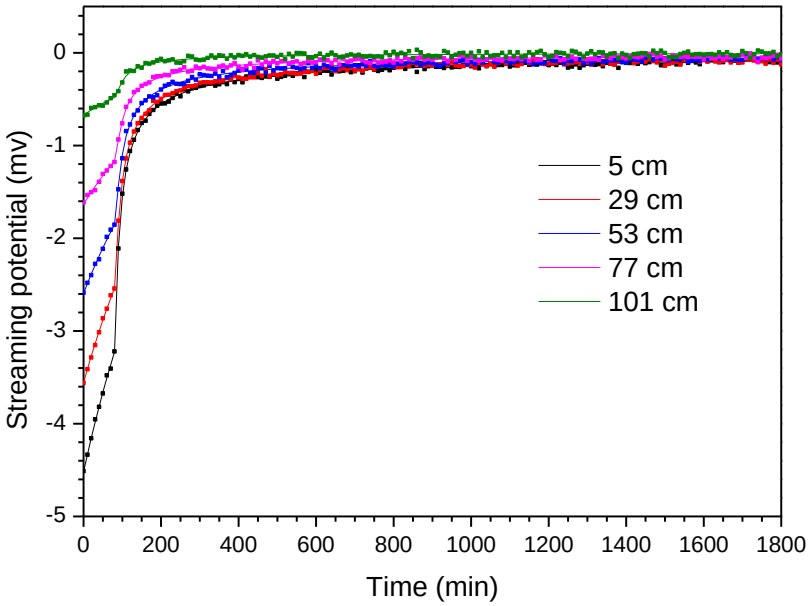

Figure 2. Reference SP signals. Solid lines represent the reference SP solution and dots represent the sets of perturbed data serving as conditioning information for model calibration.

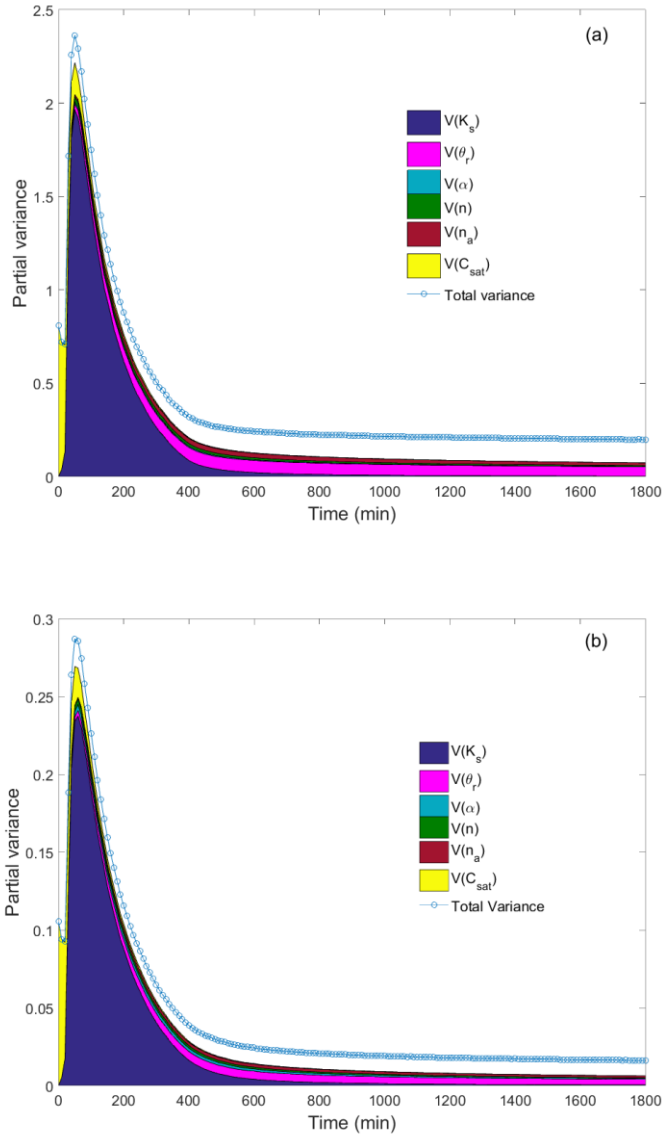

Figure 3. Time distribution of the SP variance at 5cm (a) and 77cm (b) depth. The shaded area under the variance curve represents the partial marginal contributions of the random input parameters; the contribution of interactions between parameters is represented by the blank region between the shaded area and the variance curve.

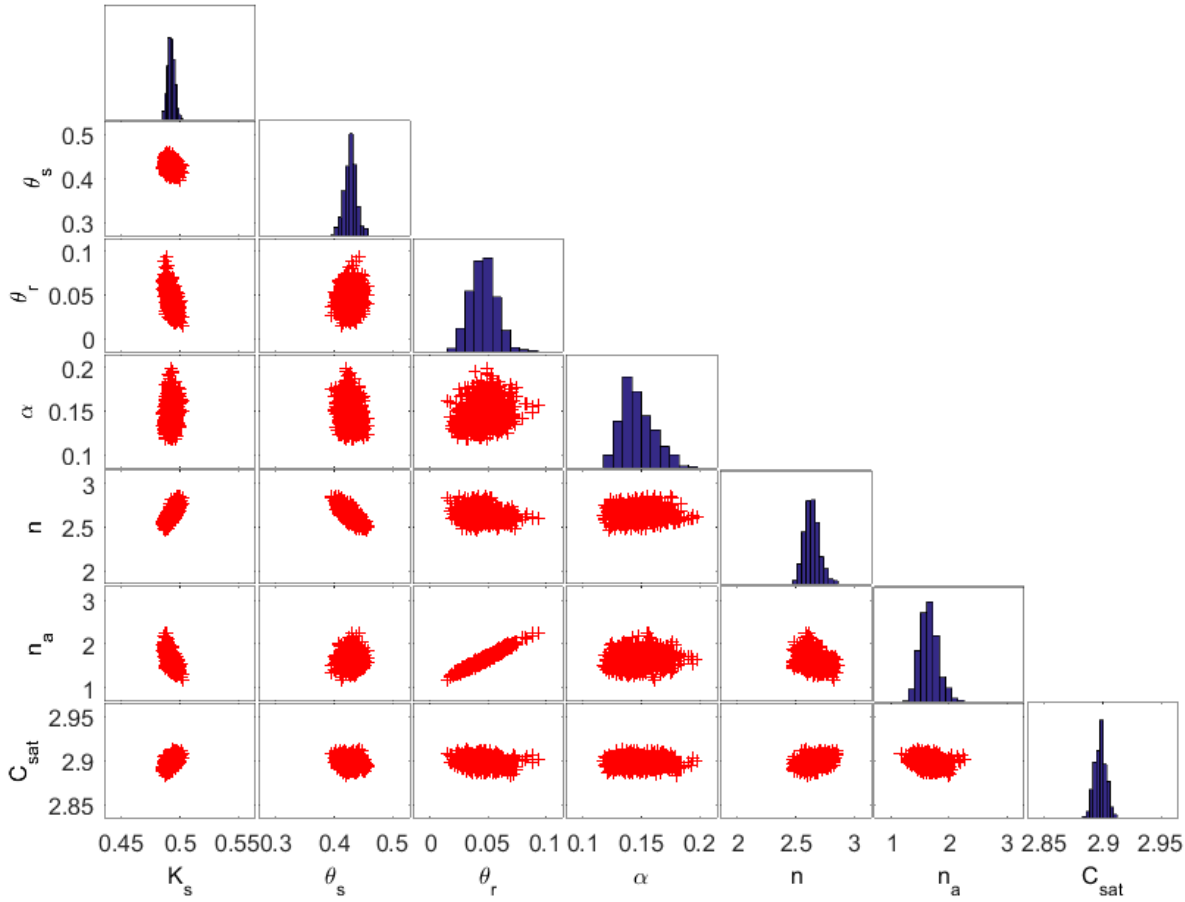

Figure 4. MCMC solutions when all SP data are considered for the calibration. The diagonal plots represent the inferred posterior probability distribution of the model parameters. The off-diagonal scatterplots represent the pairwise correlations in the MCMC drawing.

581

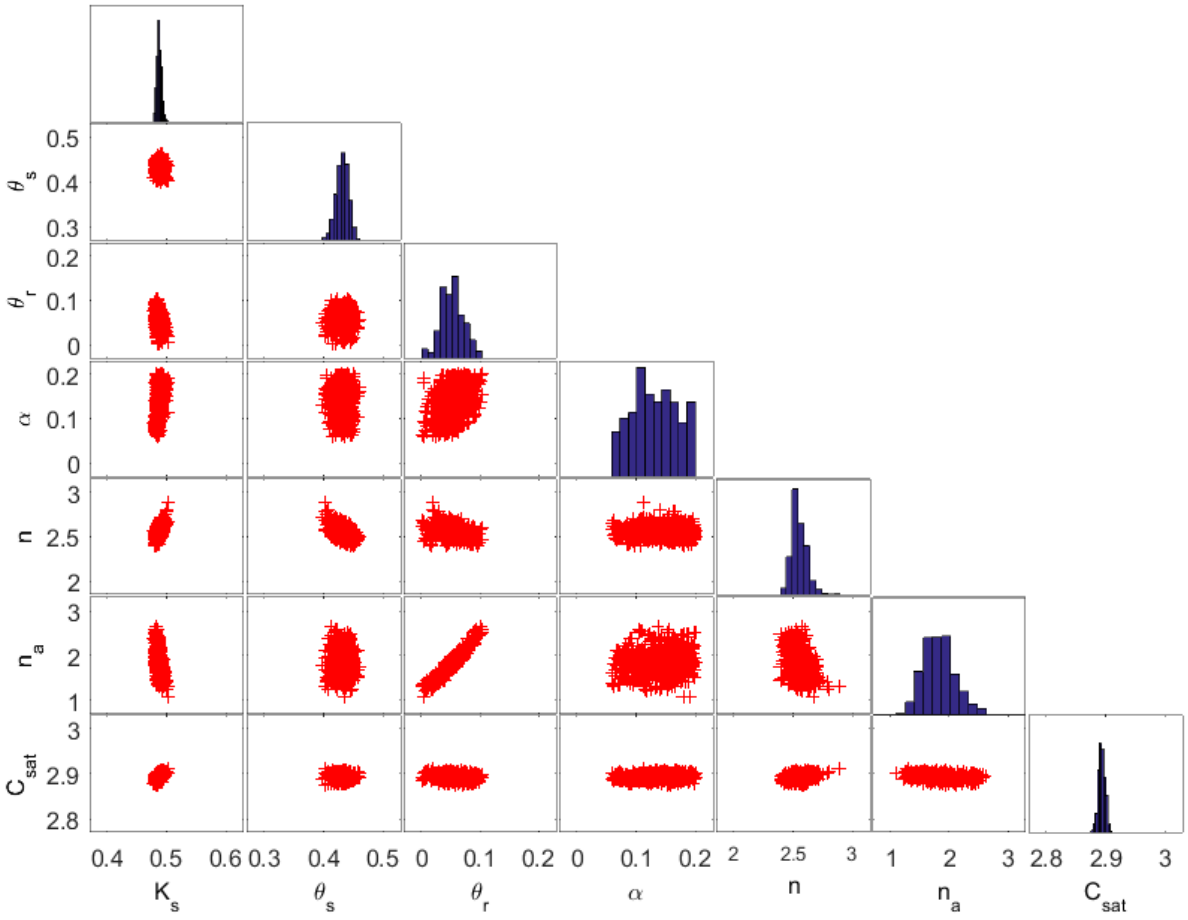

Figure 5. MCMC solutions when calibration is performed using only SP data located at 5 cm from the surface. The diagonal plots represent the posterior probability distribution of the parameters. The off-diagonal scatterplots represent the pairwise correlations in the MCMC drawing.